Influence of Material Properties and Geometric Shape of Magnetic Cores on Acoustic Noise Emission of Medium-Frequency Transformers

Peng Shuai, *Student Member, IEEE*, and Juergen Biela, *Senior Member, IEEE*

***Abstract*—Medium-voltage, medium-frequency transformers (MFTs) are much smaller in size and weight compared to conventional line frequency transformers. MFTs are very attractive for applications where full control of the power flow and high power density are required, such as power electronic interfaces in smart grids and traction converter systems. Because of the switching loss of high-voltage semiconductor switches and the limitation of volume reduction at high frequency due to isolation requirement, MFTs are usually operated in the kHz range, which results in acoustic noise emission. In this paper, the origins of acoustic noise associated with MFTs are investigated based on vibration and acoustic measurements. The work focuses on the influence of material properties and geometric shape of the magnetic core. Based on the measurement results, nanocrystalline uncut cores with oval shape is the best solution for MFT design regarding high efficiency, high power density, and low acoustic noise emission. Finally, the low acoustic noise emission of a prototype transformer built with nanocrystalline uncut cores is verified by measurement. The winding is found to have major contribution to transformer acoustic noise if the low-magnetostrictive uncut core is used.**

***Index Terms*—Acoustic noise, transformers, vibrations.**

I. Introduction

IN FUTURE, more renewable energy sources and energy storage systems will be integrated into the electric power system. Due to the inherently fluctuating properties of the renewable energy, the dynamic control of the power flow is essential. Besides the basic functions of transformers, an energy conversion interface interconnecting the medium-voltage (MV) grid and the low-voltage (LV) grid with additional features, such as LV dc link, power factor correction, reactive power compensation, active filtering, and smart protection are desired [1]. One feasible solution is the solid-state transformer (SST) as shown in Fig. 1, where multistage power electronic converters are employed to perform power conversion between the MV and LV grids. As the key parts of the SST, the isolated dc–dc converters with medium-frequency transformer (MFT) realize the galvanic isolation and voltage level matching. The dc-dc converters

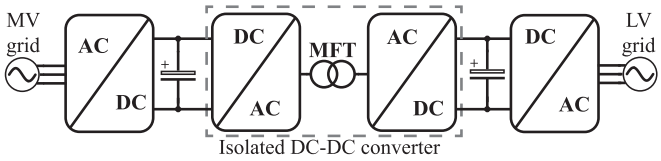

Fig. 1. Basic concept of SST.

are operated at a much higher frequency than line frequency, and therefore, the size and weight of the transformer can be significantly reduced, which is attractive for applications where the space is limited, e.g., in offshore wind farms and traction systems for locomotives. The additional functionalities of SST also enable its application in smart grid.

To reduce the size of the transformer, it is desirable to operate the dc–dc converter at higher frequency. However, for high-power applications, the operating frequency is usually in the range of a few kHz mainly due to the switching losses and the limited volume reduction at high frequencies because of the required isolation distance [2]. The operation of converters in the audible frequency range implies that the acoustic noise emission from the transformer cannot be avoided.

The acoustic noise issue of magnetic devices has been constantly investigated in the past few decades. There exist extensive studies for electrical machines [3]–[5] and for power transformers operating at line frequency [6]–[8]. However, in the medium-frequency range, literature regarding this topic is rare. The investigation of acoustic noise emission of electromagnetic components operating in the medium-frequency range are presented in [9]–[14] for inductors. In [9], a noise reduction method is proposed for inductors with distributed air gaps in iron cores by handling the frequency of free modes vibration. In [10], the noise reduction of electrical steel based inductors is achieved by reducing the flux density and modification of the air gap filler. The measurements of sound pressure level (SPL) are performed for inductors built with grain-oriented steel and ferrite cores under diverse excitation conditions in [11]. The magnetostriction and acoustic noise of Si–Fe powder compressed cores are measured in [12] for inductors employed in photovoltaic generators. In the extensive studies carried out for single-phase and three-phase inductors in [13] and [14], the authors propose to reduce the noise by improving the air gap distribution in grain-oriented steel core and by optimizing the hardness of the air gap filler. In a recent publication [15], the contribution of

Manuscript received October 19, 2016; accepted November 26, 2016. Date of publication December 7, 2016; date of current version May 9, 2017. This work was supported by the European Center for Power Electronics (ECPE). Recommended for publication by Associate Editor F. Costa.

The authors are with the Laboratory for High Power Electronic Systems, ETH Zürich, Zurich CH-8092, Switzerland (e-mail: shuai@hpe.ee.ethz.ch; jbiela@ethz.ch).

Color versions of one or more of the figures in this paper are available online at http://ieeexplore.ieee.org.

Digital Object Identifier 10.1109/TPEL.2016.2636572

magnetostriction and Maxwell force to the core deformation of inductor is investigated based on analytical method and finite element method (FEM). It has been shown that both effects can be dominant depending on the material properties and the configuration of the air gaps in the core.

Regarding transformers, the acoustic noise of several spacecraft power transformers built with Si–Fe and Ni–Fe–Mo cores are measured and compared in [16]. The study is focusing on the influences of the core types and air gap, recommendations for low noise transformer design are proposed. The dependency of acoustic noise on frequency and magnetomechanical resonance is investigated in [17] for three-phase three-limb transformers. Finally, the acoustic characteristics of three-phase transformers built with amorphous cores operating at 60 Hz are introduced in [18] and [19]. The work focuses on the influence of bending structure of cores on vibration and acoustic noise emission.

Although the sources of acoustic noise regarding line frequency transformer (LFT) are well identified and related measures to reduce the noise are also widely investigated; a reevaluation for MFT is still demanded due to the difference in used core materials, mechanical construction, and operation conditions. This paper investigates the electromagnetic origins of acoustic noise in MFTs focusing on the following aspects:

1) mechanisms causing vibrations of the tape wound cores commonly used for MFTs;
2) core materials for medium-frequency applications;
3) impact of material properties and geometric shape;
4) comparison of core vibration and winding vibration.

For MFT, the research work regarding the acoustic noise is rarely to be found. In [20] and [21], the vibration and acoustic noise measurements are performed on magnetic cores made by various materials and with different geometric shapes. This paper summarizes the results obtained in [20] and [21] and adds new acoustic measurements performed on a prototype transformer operated at 4 kHz under the excitation of rectangular shaped voltage.

II. Origins of Acoustic Noise in MFT

Acoustic noise is undesirable sound, which is the acoustic waves perceived by human ears. The vibrations of solid bodies cause the particles in the surrounding air to vibrate and generate acoustic waves. The vibrations of transformers are mainly induced by electromagnetic excitation. In some cases, noise may also be caused by the auxiliary equipments, such as fans and oil pumps, which is out of the scope of this paper. In MFTs, there are three main electromagnetic origins of vibrations:

1) the magnetostriction of the core;
2) the Maxwell force acting on the core;
3) the Lorentz force acting on the winding.

A. Magnetostriction

Magnetostriction represents the dimension change of a deformable substance due to the change of magnetization. In soft ferromagnet, magnetostriction can be obviously detected by measurement and is generally considered to be the major cause of the core vibration in transformers [8].

TABLE I
Properties of Some Magnetic Materials [23]

Material	Saturation flux density [T]	Saturation magnetostriction [μm/m]	Loss @ 0.2 T/20 kHz [W/kg]
6.5% Si–Fe (50 μm)	1.8	0	60
Mn–Zn ferrite	0.45−0.55	−2–0	10−15
Fe-based amorphous alloy Metglas 2605SA1	1.56	27	$8 \sim 10$
Co-based amorphous alloy VITROVAC 6030	0.82	<0.2	2.2
Nanocrystalline alloy VITROPERM 500F	1.2	<0.5	1.8

Magnetostriction λ is quantified by the relative change in length of the material, which is a strain represented as

$$\lambda = \frac{\Delta l}{l} \tag{1}$$

where l is the length of the material and Δl is the change of the length. The value of λ at the magnetic saturation point is called saturation magnetostriction and is represented by λ_s, which is a property of the material. Even in strong magnetic materials, the magnetostrictive effect is small: The typical value of λ_s is in order of 10^{-5}. This value can be positive, negative, or even zero in some cases. The positive value means elongation and negative value represents contraction (see Table I).

In case of soft ferromagnet used for transformers, the most relevant magnetoelastic effects for core vibration is the Joule magnetostriction [3]. For isotropic materials, the magnetostrictive strain λ_p parallel to the direction of the applied magnetic field can be calculated as

$$\lambda_p = \lambda_s \cdot \left(\frac{B}{B_s}\right)^2 \tag{2}$$

where B is the actual magnetic flux density, and B_s is the saturation flux density.

With Joule magnetostriction, the volume of the ferromagnet remains constant. This indicates that there exists a strain λ_t in the transverse directions with opposite sign, i.e.,

$$\lambda_t = -\frac{1}{2}\lambda_p. \tag{3}$$

Joule magnetostriction is not only field dependent but also related to mechanical stress σ. Therefore, it can be represented as a function of magnetic field strength H and σ, i.e., $\lambda = f(H, \sigma)$.

B. Maxwell Force

The Maxwell force (also known as reluctance force) is acting on the boundaries between two materials with different magnetic permeabilities. Regarding transformers (dry-type), these forces are presented on the core–air interfaces where the permeability changes from μ (magnetic material) to μ_0 (air). The surface density of Maxwell force in normal direction is given as

$$\vec{\mathbf{f}} = \frac{1}{2}\left[\left(\frac{1}{\mu_0} - \frac{1}{\mu}\right) B_n^2 + (\mu - \mu_0)\, H_t^2\right] \vec{\mathbf{n}} \tag{4}$$

where B_n is the normal component of the flux density and H_t is the tangential components of magnetic field strength regarding the surface. The validity of this equation is under the assumption of homogeneous fields and linear, isotropic, incompressible materials [22]. In most cases, $\mu \gg \mu_0$, therefore, the force density given by (4) is positive and points outwards the surface. For transformers constructed with laminated cores, the Maxwell forces are acting on the core surfaces including the air gaps, and also inside the core at the joints and between the stacked layers [6].

C. Lorentz Force

The Lorentz forces act on the current-conducting conductors posed in a magnetic field. Unlike the Maxwell force, the Lorentz force is a volume force and its density is calculated by

$$\vec{\mathbf{f}}_{\mathrm{v}} = \vec{\mathbf{J}} \times \vec{\mathbf{B}} \tag{5}$$

where $\vec{\mathbf{J}}$ is the current density in the conductor and $\vec{\mathbf{B}}$ is the magnetic flux density vector.

In the literature, the contribution of Lorentz force to transformer acoustic noise is usually considered to be less significant than the other two sources. However, it is concluded in [9] that the winding is always a source of mechanical stress, so it cannot be ignored in the mechanical analysis.

D. Maxwell Force and Magnetostriction in Laminated Core

As mentioned before, transformer cores used for medium-frequency applications are different in terms of material and construction from the ones used in the low-frequency range. For MFT applications, the cores are usually wound by very thin ribbons (typically 15 to 25 μm) made of amorphous or nanocrystalline alloys [23]. The thickness of the ribbons is much thinner than Si–Fe sheets used for LFTs. On the other hand, according to the manufacturing process, there exists no joints in tape wound cores. Although the air gaps are desired to be eliminated in transformers, the use of cut cores due to construction convenience still introduces very thin air gaps.

In Figs. 2 and 3, part of the rectangular shaped core including the air gap and the laminated structure of the thin ribbons are roughly shown. The magnetostriction of the core material is considered to be positive. Based on the analysis in [6], the mechanisms of magnetostriction and Maxwell force are illustrated. In the bulky region far away from the air gap, the propagation of magnetic flux lines is parallel to the ribbons. The in-plane magnetostriction causes an elongation of the ribbon along the flux line and the ribbon become thinner and narrower due to the volume conservation of Joule magnetostriction. The elongation of the ribbons also leads to the outward expansion of the core due to the increased length of the core leg. Near the air gap region, the stretched ribbons due to the in-plane magnetostriction cause the reduction of the air gap length and may lead to mechanical contact of the two parts. On the other hand, the distortion of the flux lines due to fringing field at the air gap leads to off-plane magnetostriction that induces the local increase of the lamination height as shown in the graph.

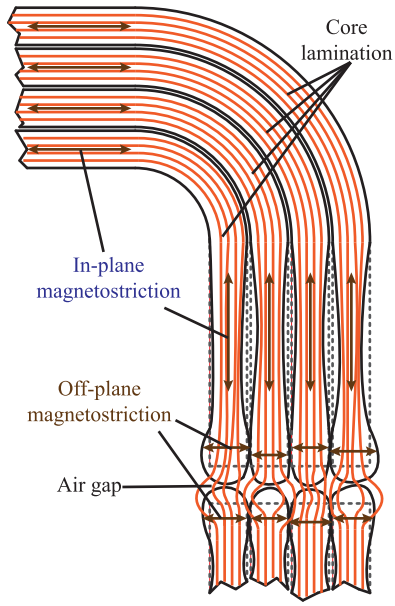

Fig. 2. Mechanisms of magnetostriction in tape wound cores.

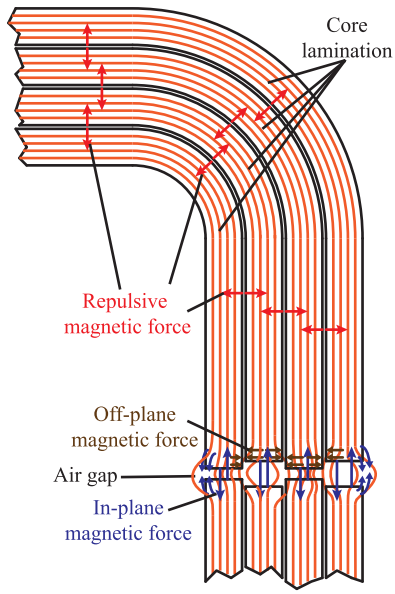

Fig. 3. Mechanisms of Maxwell force in tape wound cores.

Besides magnetostriction, the following mechanisms of Maxwell force as shown in Fig. 3 can be assumed for tape wound core:

1) repulsive forces between lamination sheets;
2) in-plane attractive forces between the sheet ends (air gap region);
3) off-plane attractive forces between the lamination sheets near the air gaps.

In the regions far away from the air gap, the repulsive forces between lamination sheets are considered to be negligibly small [6]. Therefore, the major effects of the Maxwell force are in the air gap region, where the in-plane attractive forces pull the two core parts together and the off-plane attractive force drag

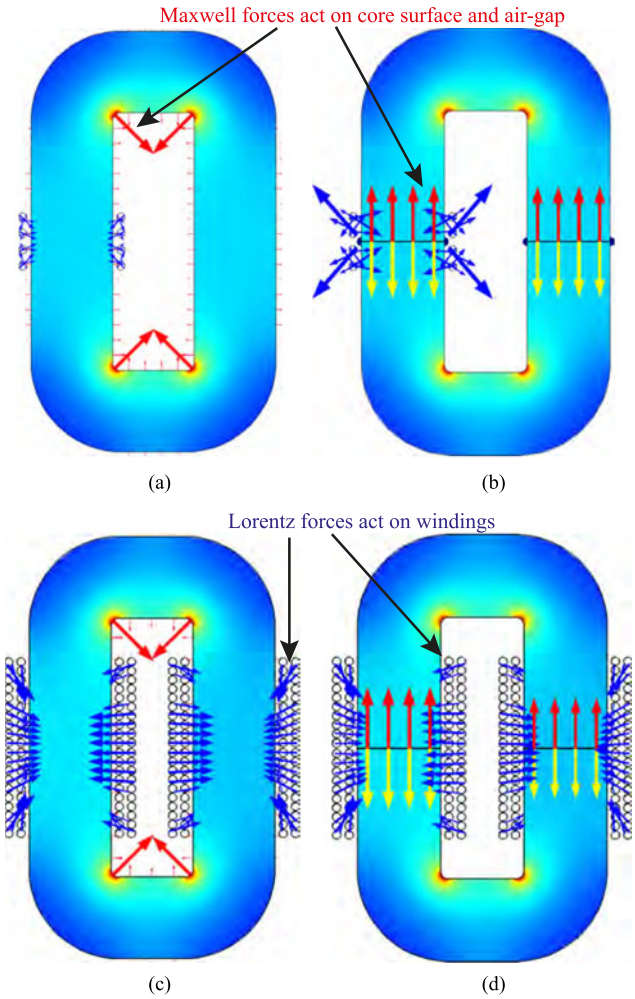

Fig. 4. Maxwell forces and Lorentz forces distribution at the same magnetic flux density in inductors and transformers with or without air gaps. (a) Inductor with uncut core: Maxwell force scale factor: 10^3; Lorentz force scale factor: 10^4; excitation current: 3.42 A. (b) Inductor with 0.1 mm air gap: Maxwell force scale factor: 1; Lorentz force scale factor: 500; excitation current: 23.32 A. (c) Transformer with uncut core: Maxwell force scale factor: 10^3; Lorentz force scale factor: 100; primary side current: 20 A; secondary side current: 19.66 A. (d) Transformer with 0.1 mm air gap: Maxwell force scale factor: 1; Lorentz force scale factor: 100; primary side current: 20 A; secondary side current: 17.7 A.

the sheets ends toward each other. The mechanism of Maxwell force and magnetostriction at the ribbon ends are linked and enhanced with each other that induce excessive vibrations of the core. Therefore, the presence of a thin air gap in case of cut core is considered to have significant contribution to the acoustic noise emission of transformers.

E. Maxwell Force Versus Lorentz Force

As mentioned before, the Lorentz force is considered to be less significant than the other two sources of acoustic noise. To compare the Maxwell force and the Lorentz force, FEM simulations are performed as case studies for inductors and transformers with cut and uncut cores. The magnetic material is set to be linear and isotropic with a relative permeability of 10 000. In all cases shown in Fig. 4, the cores are excited to the same peak flux density (0.5 T) in the middle of the core limbs and around 1.5 T at the inner corners. The simulation is performed for the static case considering a sinusoidal current excitation at the instance of peak value. The inductor winding has 4 turns and the transformer winding has 40 turns (turns ratio 1:1). The current in the transformer primary winding is almost ten times higher than the current in inductor winding that results in much larger Lorentz forces acting on the transformer winding. If no air gap exists, the Maxwell force is distributed around the core with high amplitudes at the inner corners due to the locally high flux density. The Lorentz force is comparable to Maxwell force, especially for the transformer. In case that air gaps exist, the attractive force at the air gap is dominant and is much more significant than the Lorentz force.

III. Core Materials for MFT Applications

To realize a transformer with low acoustic noise emission, a suitable core material is essential. Therefore, a material with low iron loss, high saturation flux density, and also with small magnetostriction is preferred. In Table I, the relevant properties of several magnetic materials are listed.

Among these materials, Si–Fe has the highest saturation level. Although the loss of this material is significantly higher, it is widely used for low-frequency large-power transformers due to the relative low price. With the silicon weight percentage of 6.5%, the magnetostriction of Si–Fe is nearly zero, which is advantageous to reduce the acoustic noise. In the medium-frequency range, the iron loss of Si–Fe becomes too high due to the eddy current loss, which prohibits its utilization as transformer core. The application of ferrite is typically above 20 kHz due to its low saturation level.

In medium-frequency range, the commonly used core materials for transformers are amorphous and nanocrystalline alloys. Depending on the composition of the alloy, the properties of the material are significantly different. Fe-based amorphous alloys, such as Metglas 2605SA1 are composed of low cost raw materials, e.g., Fe, Si, and B. The high content of Fe enables high saturation flux density of the alloy which is comparable to Si–Fe while the core loss is significantly lower. However, the large magnetostriction of Fe-based amorphous alloy is obviously a drawback considering acoustic noise emission. By adding additional contents including Co and reducing the percentage of Fe, the specific loss of the amorphous alloys is reduced but the saturation level is also lower. Depending on the Fe/Co ratio, the saturation flux density of Co-based amorphous alloys can vary from 0.4 to 1 T. By carefully controlling this ratio, nearly zero magnetostriction can be achieved, which is very attractive for acoustic noise reduction [23]. Nevertheless, Co-based amorphous alloys are seldom to be found for MFT applications due to the high material cost.

Fe-based nanocrystalline alloys, e.g., VITROPERM 500F, are composed of Fe, Si, B, Cu, Nb, etc. The saturation level of this material is relative high and the specific loss is the lowest among the listed materials. Similarly, the Si content can be controlled at around 15–16 at% (atomic percent) so that a near-zero magnetostriction can be achieved after nanocrystallization [23]. The combination of these properties apparently shows the suitability of nanocrystalline alloy as core material of transformers

TABLE II
DIMENSIONS OF CORES FOR MEASUREMENT

Core Size [mm]	A	B	C	D	W	H
VAC VITROPERM 500F T60102-L2157-W159 (reference of size)	29.6	30	95	26.6	90	157.5
Metglas 2605SA1 PS0509CA	28.6	30	95	30	87.2	152.2
Kaschke K2008 U93/30/76	28	34.6	96	30	93	152

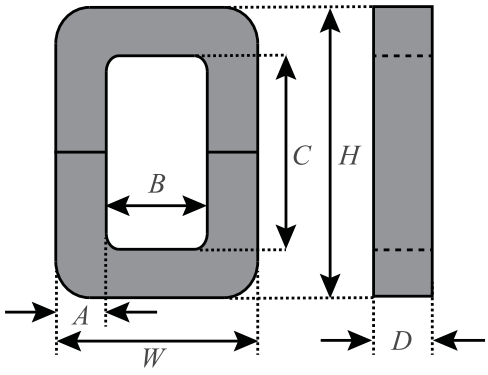

Fig. 5. Rectangular core dimensions.

for medium-frequency, MV applications. The only drawback of this material is the relative high cost.

IV. VIBRATION AND ACOUSTIC MEASUREMENTS OF MAGNETIC CORES

To compare different core materials and geometric shapes regarding the vibration and acoustic noise emission, experimental measurements are performed on several cores with similar size.

A. Sample Cores

For the measurements, two standard nanocrystalline (VITROPERM 500F) cores T60102-L2157-W159 with rectangular shape from VACUUMSCHMELZE are selected as the reference of size. One of the core is cut in the middle and another one is uncut. For comparison of different materials, a Fe-based amorphous cut core with the material Metglas 2605SA1 and a ferrite cut core from Kaschke with the material K2008 are chosen. The dimensions of these cores are listed in Table II with the parameters shown in Fig. 5.

To compare the impact of the geometric shapes, an oval core and a ring core are also considered. Both cores are uncut, made by VITROPERM 500F and have the same tape width, cross-sectional area, and similar magnetic length as the reference core. The three nanocrystalline cores and the measured dimensions are shown in Fig. 6. Due to the manufacturing tolerance, the dimensions of the rectangular core are slightly different to the values given in Table II and the core leg width (A) of the three cores in Fig. 6 has a difference of ± 1 mm.

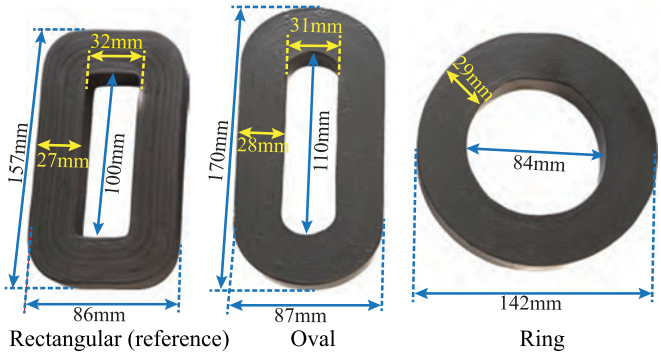

Fig. 6. Nanocrystalline cores and their measured dimensions.

B. Measurement Setup

The measurement setup as shown in Fig. 7(a) has been built for both the vibration and the acoustic noise measurements. The excitation voltage/current for the cores is generated by a signal generator, amplified with a power amplifier and then fed to the excitation winding of the core. A capacitor bank with a total capacitance of 5mF is connected in series to decouple the dc component that might be introduced by the power amplifier. To control the excitation voltage and obtain the desired magnetic flux density in the core, a measurement winding is added. The voltage on this winding is measured by the digital multimeter (NI PXI-4071) and sent to the PC as feedback signal to regulate the output voltage of the signal generator by using the NI LabVIEW software.

The vibration of the core is measured with a laser scanning vibrometer (Polytec PSV-400) controlled by the Polytec OFV-5000 controller, which allows a noncontact measurement without mechanical influence on the core as in the case of using a contact-type accelerometer. The core is placed on a vibration isolated table to avoid the disturbance from the environment. The measured signal is decoded to velocity and acquired by the data recorder and sent to the PC for further analysis.

The acoustic measurement is done by measuring the SPL through an 1/4-in microphone with integrated preamplifier (G.R.A.S. 40PH), where the measured signal is acquired by the dynamic signal analyzer (NI PXI-4462) and then sent to the PC. The core is located in the center of an anechoic room with dimensions much larger than the core. The microphone is located 1 m away from the surface of the core.

The vibration measurements are performed on three surface areas of the magnetic cores as indicated in Fig. 7(b), i.e., side, top, and front surfaces. Accordingly, the acoustic measurements are also performed separately from x, y, z-directions. For the ring core, only two surfaces are measured due to its symmetry. During both vibration and acoustic measurements, the sensor (vibrometer or microphone) is fixed at the same location while the core is moved in order to measure each surface/direction. The desired peak flux density B_m is obtained by providing the calculated excitation voltage U according to

$$U = \sqrt{2}\pi f_s N_w B_m A_{\text{eff}} \tag{6}$$

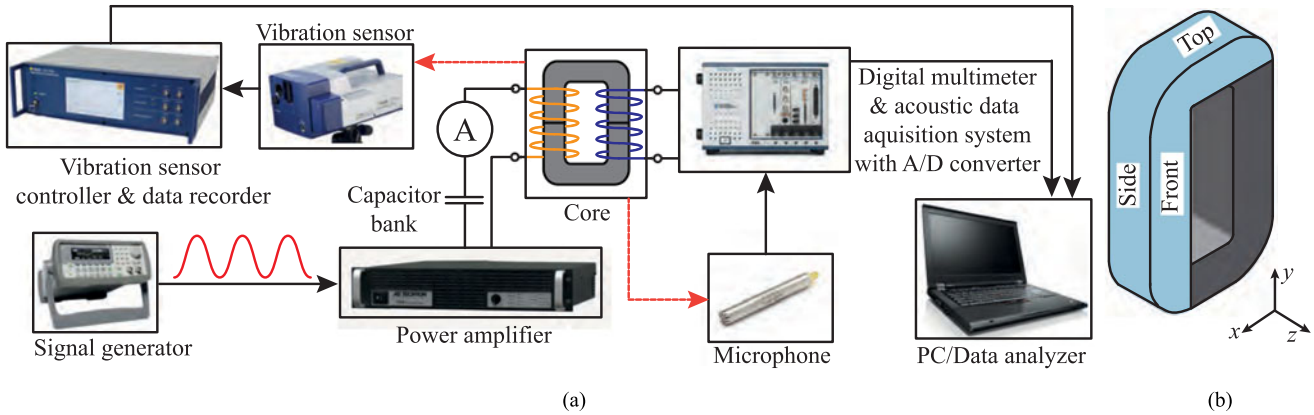

Fig. 7. Setup for vibration and acoustic noise measurement and the surface areas of the core to be measured. (a) Schematic of measurement setup. (b) Measured area.

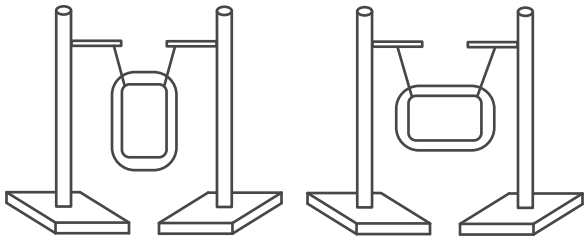

Fig. 8. Vibration measurement setup for eigenmode analysis.

where f_s is the frequency, N_w is the number of turns of the excitation winding, and A_{eff} is the effective cross-sectional area of the core given in the data sheet.

V. Measurement Results of Magnetic Cores

The vibration and acoustic measurements are performed separately with different cores excited by sinusoidal voltages/currents. The results are analyzed and discussed below.

A. Eigenfrequencies and Mode Shapes of the Rectangular Uncut Core

To investigate the eigenmode of the magnetic core, the vibration of the VITROPERM rectangular uncut core is measured by means of a frequency sweep. The core is hanging as shown in Fig. 8 to enable a "free" vibration condition. The top surface is measured by turning over the core for 90°. The excitation voltage of the core is a chirp signal. To avoid an *LC*-resonance between the capacitor bank and the magnetizing inductance, the frequency sweep is started from 300 Hz and performed up to 20 kHz. Since the flux density is lower at higher frequencies with the same amplitude of excitation voltage, the induced magnetic force is also reduced with the increase of the frequency. In order to have an obvious mechanical response of the core in the whole measuring frequency range, the frequency sweep is divided into three subranges with different amplitudes of excitation voltage: from 300 Hz to 5 kHz with 2 V, from 5 kHz to 10 kHz with 20 V and from 10 kHz to 20 kHz with 40 V.

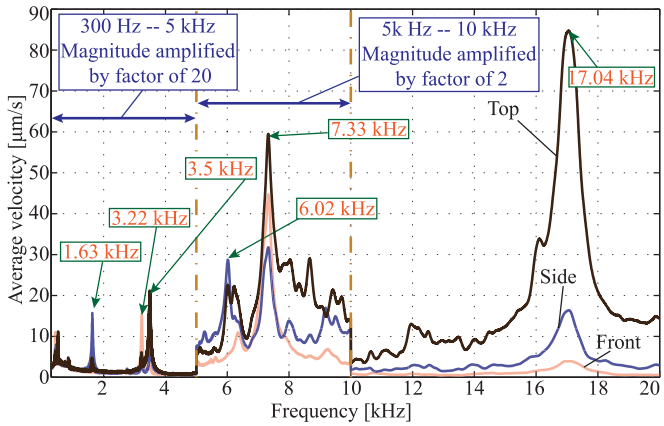

Fig. 9. Frequency spectrum of measured average surface velocity of VITROPERM rectangular uncut core by means of frequency sweep. Eigenfrequencies are indicated with the numbers.

The scanning vibrometer measures a set of points located on the measured surfaces.[1] The vibration in the direction perpendicular to the surface at these points are measured. In Fig. 9, the frequency spectra of the measured average velocity of each selected surface area are shown. To have a better visibility, the magnitudes of velocities from 300 Hz to 5 kHz and from 5 kHz to 10 kHz are multiplied by a factor of 20 and 2, respectively. As can be seen from the frequency response, several eigenfrequencies of this core are within the audible frequency range and may coincide with the frequencies of the excitation voltage and its harmonics and result in mechanical resonance. The comparison of the measured amplitude for different surfaces evidently shows that above 5 kHz the top surface has the most significant vibration, followed by the side surface whereas the vibration on the front surface is relative weak. This indicates that the tape wound core is more prone to vibrations in the directions perpendicular to the lamination layers. Since the tape wound core is composed of magnetic ribbons isolated by epoxy resin between

[1]The laser vibrometer measures the velocity in the direction of the laser. For curved surface, the measured velocity is not equal to the normal velocity of the surface.

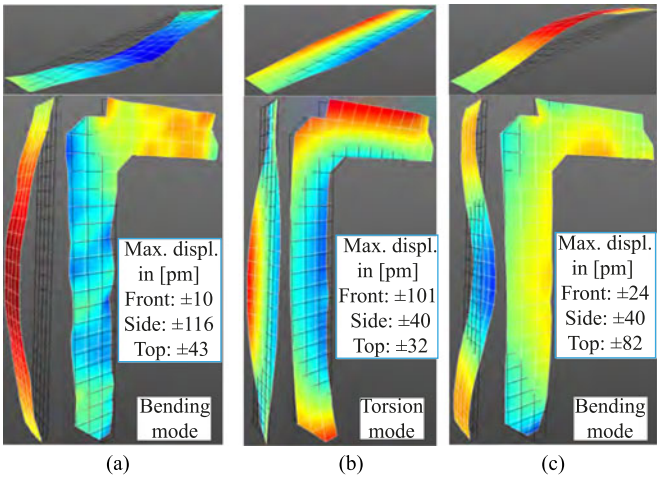

Fig. 10. First three dominant eigenmodes of VITROPERM rectangular uncut core identified from vibration measurement. The maximal displacements on each surface are indicated. (a) Mode shape at 1.63 kHz. (b) Mode shape at 3.23 kHz. (c) Mode shape at 3.5 kHz.

the lamination layers, the mechanical properties of the core is anisotropic. As introduced, e.g., in [5], the laminated core can be approximated by an orthotropic structure where the in-plane (lamination layer) material properties are assumed to be homogeneous while the material exhibits different properties in the directions perpendicular to the lamination layers.

In case of the rectangular core, the vibrations measured on side and top surfaces are mainly dependent on the out-of-plane properties whereas the vibration on front surface is mainly related to the in-plane properties. As illustrated in Fig. 10 for the first three dominant eigenmodes identified by measurement, similar mode shapes are observed on the side and top surfaces which are different as the mode shapes on the front surface. The first and third mode shapes illustrate the flexure deformation of the core limbs and yokes whereas the second mode shape shows the torsional deformation. At higher frequencies, the mode shapes are mixed with low-order vibration modes and cannot be clearly distinguished.

B. Comparison of Core Materials

To compare the influence of material properties, the vibration and acoustic noise emission of the magnetic cores listed in Table II are measured. During the measurement, all the cores are placed directly on the table without any additional mechanical mounting. In Fig. 11, the measured average surface velocities and sound pressures of these cores under excitation of 4 kHz sinusoidal voltage are shown. Since only the harmonics in audible range are of interest, all the results are rms values calculated from the first to fifth harmonics.

The comparison between the VITROPERM cut and uncut cores indicates that the vibrations are amplified by a factor of more than 10 while the sound pressure is 20 to 30 dB higher in case air gaps are present. Due to the contact of the two core parts induced by the mechanisms shown in Figs. 2 and 3, the enhancement of the vibration is quite significant especially on the top surface. Although the cut cores are preferred for transformers due to the convenience of construction, they are acoustically unfavorable [16].

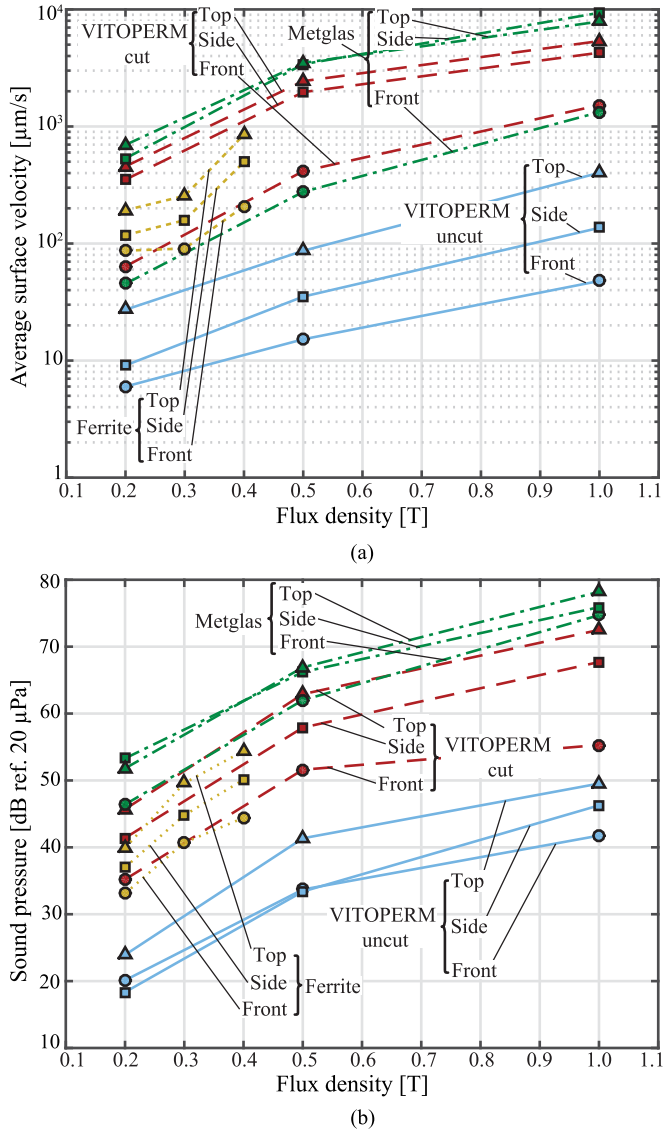

Fig. 11. Measured average surface velocities and sound pressures of magnetic cores based on different materials under excitation of 4 kHz sinusoidal voltage (only harmonics up to 20 kHz are taken into account). (a) Vibration. (b) Sound pressure.

The comparison of the cut cores made by different materials shows that the Fe-based amorphous core do have stronger vibration and more acoustic noise emission than the other two materials due to the significantly larger magnetostriction. The ferrite core is only measured at low flux density level but it can be seen that the vibration and noise emission is less than the two cut cores. Since the magnetostriction of Mn–Zn ferrite is small and negative, it causes a contraction of the core limbs. Therefore, the magnetostrictive deformation at the air gap region is in the opposite direction to the Maxwell force. These two effects are assumed to be partly canceled with each other and cause less vibration.

Further comparison among the different surfaces/directions for each individual core generally show the same relations of vibration and noise emission: top > side > front surface, which has already been shown in the frequency sweep results. The weak vibration on the front surface is mainly due to the smaller

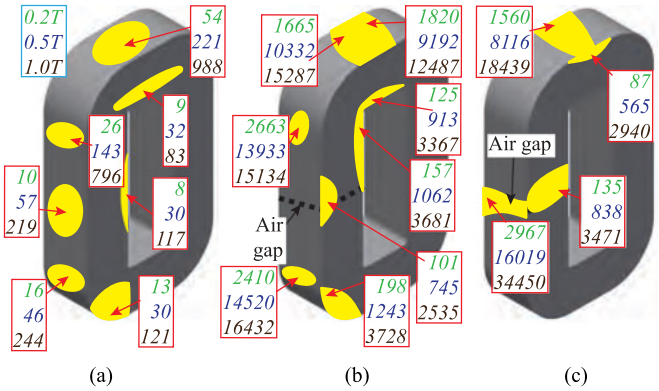

Fig. 12. Areas with relative high surface velocity on measured surfaces of nanocrystalline and amorphous cores excited by 4 kHz sinusoidal voltage. The numbers indicate the points with maximum surface velocity (rms value) in [μm/s] calculated from first to fifth harmonics for B=0.2, 0.5, 1.0 T. (a) VITROPERM uncut core. (b) VITROPERM cut core. (c) Metglas cut core.

magnetostrictive strain. Since the z-direction is perpendicular to the magnetic flux, the magnetostrictive strain is only half of the value in field direction according to (3). Also, the dimension of the core in z-direction is relative small (i.e., the thickness D in Fig. 5) compared with the x, y-directions. According to the definition (1), the magnetostrictive deformation is also small. The stronger vibration on the top surface compared to the side surface is caused by larger magnetostrictive deformation since the length $B > C$ (see Fig. 5). In case of cut cores, the contact of the core parts at the air gaps enhances the vibration in y-direction and also causes more vibration in x-direction. The difference of vibration intensity between the perpendicular and parallel directions of the lamination layers is more apparent. It should be pointed out that the measured surface velocity indicate the vibration on the measured surfaces whereas the measured sound pressure in one direction is mainly due to the acoustic waves emitted from the surface perpendicular to this direction, but the acoustic waves generated from other surfaces also have impact on the measurement results.

For more detailed analysis, the areas with relative large magnitude of surface velocity on the measured surfaces of each core are roughly depicted in Fig. 12. Here the vibrations of the highlighted areas are not in phase, i.e., the deformation of these areas do not appear at the same time. The values only represent the highest amplitudes of the measured surface velocity in the areas. On the top surface, the area with the largest vibration is located in the middle of the measured surface, which is the same for all three cores. This is related to the bending mode of the yoke as shown in Fig. 10. On the front surface, the intensive vibration appears on the corner as shown for VITROPERM cores and is related to the torsion mode [see Fig. 10(b)]. On the side surface, the bending areas (near the corners) are subject to strong vibrations, which is related to the bending mode of the core limb [see Fig. 10(c)]. The vibrations in these areas are amplified by the air gap forces in case of cut cores. These forces also cause strong vibrations in the regions near the air gaps. It can be noticed that the vibrations measured on the upper side and lower side half cores are not symmetric. The reason is that the vibration of the lower side half core is influenced by the gravity of the upper side half core and also the friction with the surface of the table.

TABLE III
COMPARISON OF VIBRATION AND SOUND PRESSURE MEASUREMENT RESULTS FOR FERRITE AND VITROVAC CORES UNDER EXCITATION OF 4 KHZ SINUSOIDAL VOLTAGE TO 0.4 T

Core	Average surface velocity (μm/s)			Sound pressure (dB ref. 20 μPa)		
	Front	Side	Top	Front	Side	Top
Ferrite	192.6	255.6	851.5	44.4	50.1	54.4
VITROVAC cut	351.2	735.7	N/A	46.7	56.8	N/A
VITROVAC uncut	3.3	3.9	N/A	−16.2	2.5	N/A

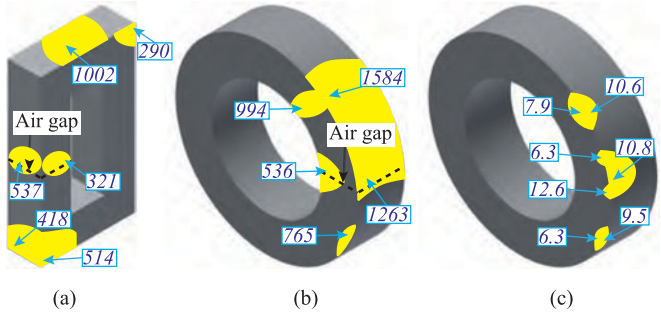

Fig. 13. Areas with relative high velocity on measured surfaces of ferrite and VITROVAC cores excited to flux density of 0.4 T with 4 kHz sinusoidal voltage. The numbers indicate the points with maximum surface velocity (rms value) in [μm/s] calculated by first to fifth harmonics. (a) Ferrite core. (b) VITROVAC cut core. (c) VITROVAC uncut core.

The Co-based amorphous alloy VITROVAC 6025Z has the same saturation magnetostriction as VITROVAC 6030 as given in Table I but a lower saturation flux density (0.58 T). Magnetic cores made of this material are not commercially available in rectangular shape. Therefore, a pair of cut and uncut ring cores with dimensions of O.D. $\times$ I.D $\times$ H $=$ 90 mm $\times$ 51 mm $\times$ 25 mm are measured for comparison. The measurement results of the cores under excitation to 0.4 T are listed in Table III and shown in Fig. 13 to compare with the ferrite core. As can be seen, the ring cores also present larger vibration/noise emission in the direction perpendicular to the lamination layers. The uncut ring core shows extremely weak vibration as well as low noise emission due to the near-zero magnetostriction of the material. On the other hand, the cut core shows more vibration and noise emission compared to the ferrite core. In this case, the vibration can be assumed mainly due to the forces around the air gap. Since the size and weight of VITROVAC cores are smaller compared to other cores, the upper half core part is more prone to vibrations.

According to the sensitivity of human ears in frequency range, the evaluation of sound source is usually done by scaling the SPL with the A-weighting curve. As an overall comparison of these cores, the A-weighted SPL averaged by the measured sound pressure from the three directions are shown in Fig. 14. The measured background noise is approximately 30 dBA in the anechoic room.

As can be seen, there is no general rule regarding the dependency of SPL on excitation frequency. The difference of dBA value can be quite significant when excited at different

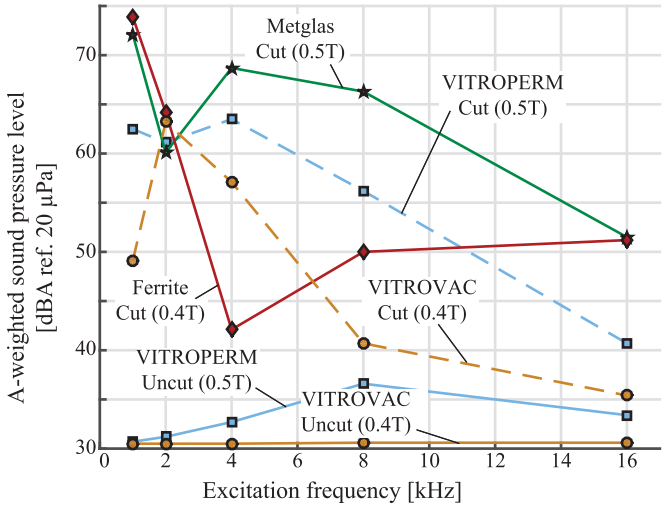

Fig. 14. A-weighted SPL of cores made by different materials under excitation of sinusoidal voltage at various frequencies.

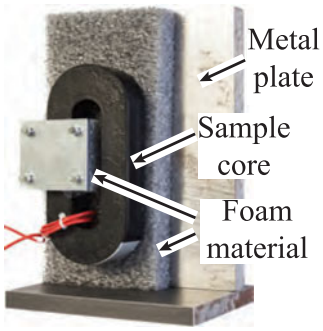

Fig. 15. Mechanical setup used for vibration measurement of nanocrystalline uncut cores.

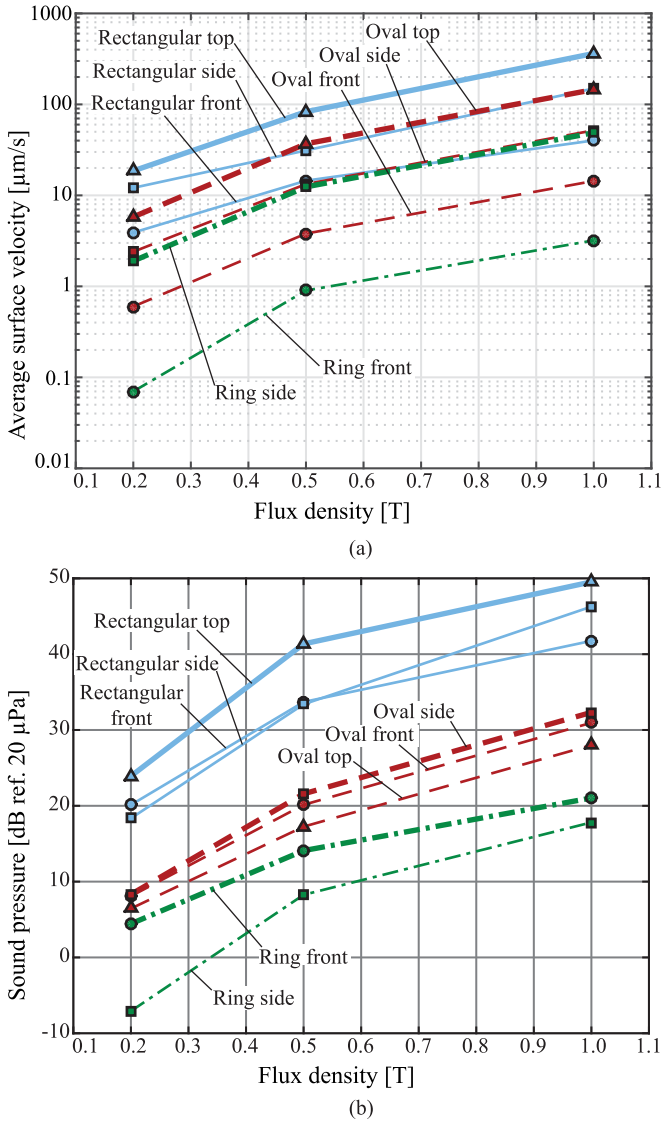

Fig. 16. Measured surface velocities and sound pressures of nanocrystalline uncut cores with different shapes under excitation of 4 kHz sinusoidal voltage (only harmonics up to 20 kHz are taken into account). (a) Vibration. (b) Sound pressure.

frequencies, which is strongly related to the resonant frequencies of each individual core. The noise level of the two uncut cores are lower than the cut cores at the measured excitation frequencies. Especially for the VITROVAC ring core, the measured SPL is close to the noise level of the background.

C. Comparison of Geometric Shapes

To compare the influence of the geometric shape, the three nanocrystalline uncut cores are measured. During the vibration measurement, an additional setup as shown in Fig. 15 is used to mount the cores, where a part of the core is fixed on a metal plate with relative large weight compared to the cores. To reduce the mechanical influence from the setup, soft foam materials are inserted between the sample cores and metal plate for damping. During the acoustic measurements, the mechanical setup is removed to avoid its reflection of the sound waves.

In Fig. 16, the measured average surface velocities and sound pressures are shown. Similar as the previous results, it could be concluded that the vibration in lamination direction is obviously stronger than in the parallel directions to the laminations regardless of the geometric shape. The comparison of velocities on each surface among these cores shows that the vibration intensity has the following relation: rectangular core $>$ oval core $>$ ring core. The measured sound pressure also confirms this relation as shown in Fig. 16(b).

The comparison among the different surfaces/directions for each individual core is already shown for the rectangular core, i.e., top $>$ side $>$ front surface for vibration/noise emission. This relation is still valid for the oval and ring cores in terms of vibrations. However, it is not valid for sound pressure. For these two cores, the lowest sound pressure is measured toward the curved surfaces on which the highest vibration velocities are detected. This is assumed to be caused by the scattering of sound waves emitted from curved surface, which propagate toward different directions. In contrary, the emitted sound waves from a flat surface mainly propagate toward the normal direction of the surface, i.e., toward the microphone.

For the analysis in the frequency domain, the harmonics of the average vibration velocities in the audible frequency range

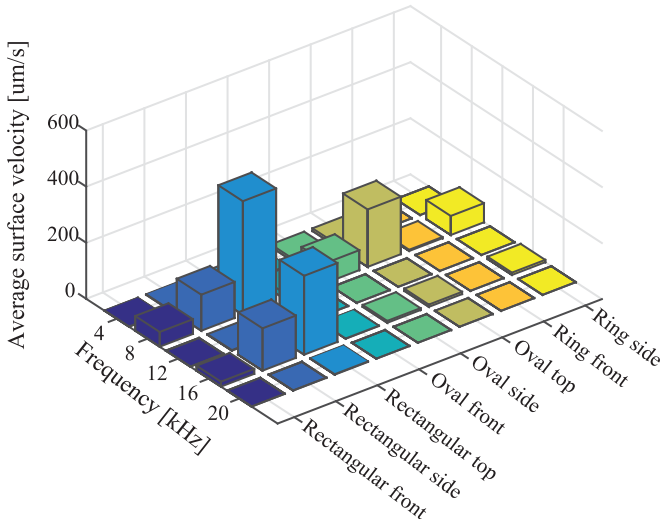

Fig. 17. Harmonics (up to 20 kHz) of average surface velocity of nanocrystalline uncut cores with different shapes under excitation of 4 kHz sinusoidal voltage at 1 T.

are shown in Fig. 17, where the measurement results at 1 T are shown. It can be seen that the major contribution of vibration is from the 8 and 16 kHz harmonics, which are the first and second harmonics of magnetostriction. The first harmonic is usually dominant and has the major contribution to acoustic noise generation. Accordingly, the deformation of the cores due to the 8-kHz harmonic at the instance when the maximum positive displacement (toward the laser) appears are shown in Fig. 18. Due to the small magnetostriction of the nanocrystalline material, the maximum deformation is within a very low range (< 20 nm) even at this high flux density level.

The A-weighted SPL of the nanocrystalline uncut cores excited to 1 T at different frequencies are shown in Fig. 19. As indicated in the graph, the ring core features the lowest acoustic noise emission at all measured frequencies. The SPL of the oval core is a few dB higher than the SPL of the ring core but lower than the SPL of the rectangular core. All three cores show obviously higher noise emissions under excitation at 8 kHz that might be due to the mechanical resonance.

D. Vibration and Acoustic Noise of Winding

To compare the vibration of the winding with the vibration of the core, measurements are performed on part of the front and top surfaces of the VITROPERM rectangular uncut core as well as on the surface of one turn of the four-turn excitation winding. For this setup, the results of some points on the front surface shown in Fig. 20(a) indicate that the measured surface velocity of the winding and the core are in a comparable range. It should be pointed out that the winding and core are mechanically coupled in this case. Therefore, the core vibration also has an influence on the winding vibration.

On the other hand, the vibration velocity on the top surface of the core shown in Fig. 20(b) is much higher than the winding vibration velocity, which is in the range of the measured values shown in Fig. 20(a). As already shown in the core measurement results, the vibration on the front surface of the core is relatively weak. Therefore, the vibration of the winding is relatively small compared with the vibration of core in case that a relative low current (e.g., inductor built with uncut core) is flowing through the winding.

In case of a cut core excited to the same flux density level, the magnetizing current is larger, and the Lorentz force acting on the winding also increases. Furthermore, transformer windings usually conduct a high current, which also results in a large Lorentz force (see Fig. 4). In Fig. 21, the vibration and the sound pressure measured on a winding constructed with 60 turns of Litz-wire (620×0.1 mm, 3 layers, 20 turns per layer) fed by 20A peak sinusoidal current are shown. It can be seen that the maximal vibration velocity can reach over 200 μ/s, which is in the range of the nanocrystalline uncut core vibration velocity as shown in Fig. 20(b). In case that the core vibration is relative large, e.g., Metglas cut core (see Fig. 12), the surface velocity in some areas can reach over 10 mm/s, which is much higher than the measured winding velocity in this case.

The measured sound pressure of the winding shown in Fig. 21(b) indicates that the A-weighted SPL is 50 dBA, where the first harmonic is dominant in the frequency spectrum. In this case, the amplitude of the current is much higher compared to the excitation current during the uncut core measurement. Consequently, the noise of the winding is higher than the nanocrystalline uncut core excited to 1 T at 4 kHz as shown in Fig. 19. Therefore, it can be concluded that the vibration of winding can be considered to have minor contribution to acoustic noise emission of transformers only if the core vibration is relative large and the current in the winding is relative small. This is also mentioned for large power transformers with low induction level and improved core designs, where the load current dependent winding vibration can have significant contribution to the transformer noise [24].

E. Discussion About the Harmonics of the Vibration

In case of a pure ac sinusoidal excitation, the winding current/voltage of transformer only contains a single harmonic at the excitation frequency. Theoretically, the magnetostriction and Maxwell force are proportional to the square of flux density whereas the Lorentz force is proportional to the square of current. Therefore, the vibration signal should only contain a single harmonic at twice of the excitation frequency. However, measurement results show that the frequency spectra of the vibration velocities and the sound pressures contain harmonic at excitation frequency and higher-order harmonics, which are present in both core and winding measurement results. Due to the hysteresis between the flux density B and the magnetic field strength H, the magnetostriction and the electromagnetic force contain also higher-order harmonics (normally odd harmonics) [25], [26], which lead to higher order even harmonics (due to the square relation) in the vibration signal, e.g., 8, 16, and 32-kHz harmonics by 4 kHz excitation. Furthermore, odd harmonics (e.g., 4, 12, and 20 kHz) are also detected in the measured vibration signal, for both core and winding.

1) Magnetic Core: In case of the core vibration, the odd harmonics can be caused by dc magnetization, which leads to an

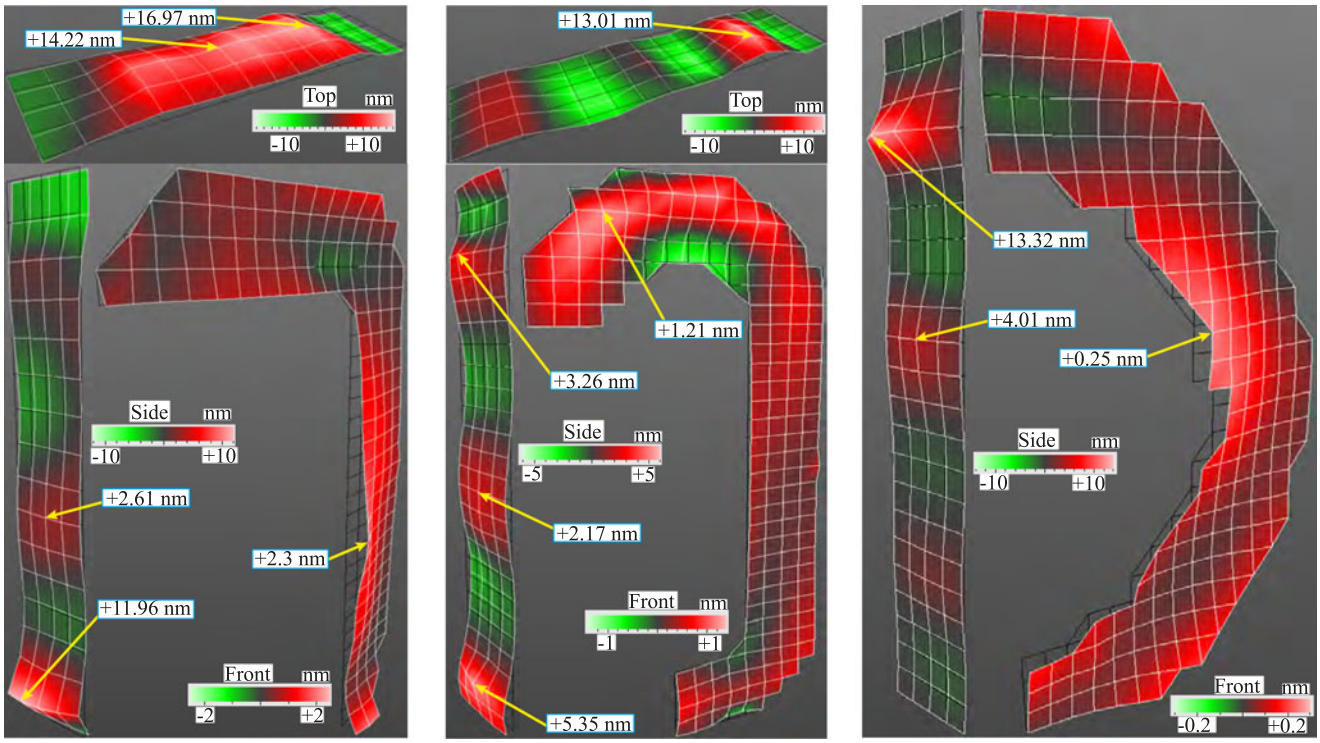

Fig. 18. Snapshot from vibration animation of 8-kHz harmonic at the instance when cores show maximum outward deformation (toward the laser) under excitation of 4 kHz sinusoidal voltage to 1 T. (a) Rectangular core. (b) Oval core. (c) Ring core.

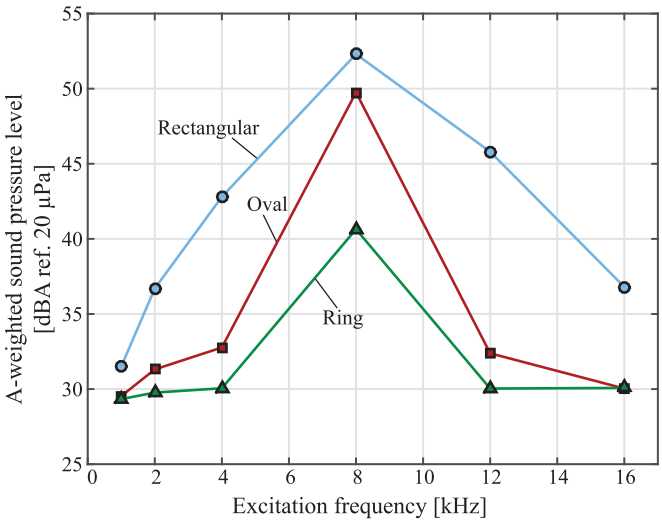

Fig. 19. A-weighted SPL of nanocrystalline uncut cores with different shapes under excitation of sinusoidal voltage to 1 T at various frequencies.

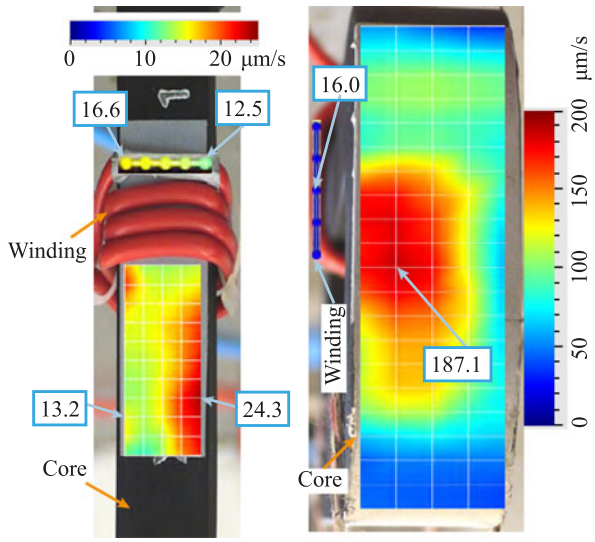

Fig. 20. Comparison of measured velocities of the winding and the VITROPERM uncut core excited to 0.5 T at 4 kHz. (a) Front. (b) Top.

asymmetrical magnetostriction within one magnetization cycle [27]. This phenomenon is well known for large power transformers, where even a small dc magnetization of the core can lead to a significant increase of the vibration [24].

Even if there is no dc magnetization, asymmetrical magnetostriction may still exist. As presented in [28], the symmetry of magnetostriction is obtained only if the direction of the applied magnetic field and the magnetic equivalent easy axis (EEA) of the ribbon is perpendicular or parallel. In both cases, the symmetry (or the even condition of magnetization variation) is fulfilled and the magnetostriction only contains even harmonics. Otherwise, the symmetry of magnetostriction is broken that results in odd harmonics. In practice, the magnetic flux lines are not in parallel to the ribbon axis (which is usually parallel to the EEA of the ribbon after thermal annealing in a magnetic

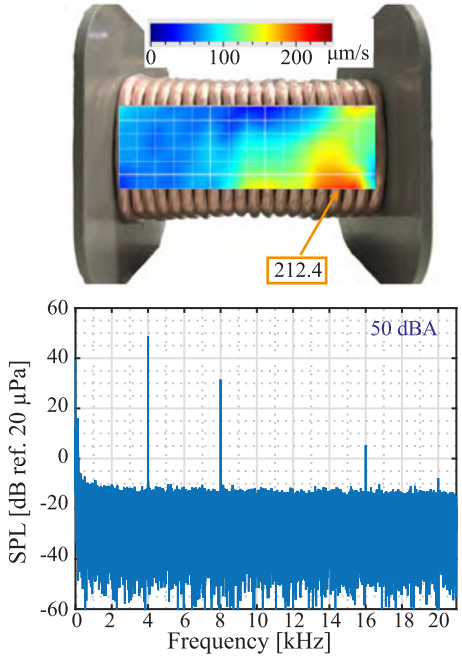

Fig. 21. Measured vibration velocity and sound pressure spectrum of a winding constructed with round Litz-wire.

field) at some locations of the core. Consequently, the symmetry condition of magnetostriction is broken in these locations. This effect is frequency dependent. At very low frequencies, there exists the frequency doubling effect of magnetostriction. With the increase of frequency, the distortion of the magnetostriction becomes more significant and odd harmonics appear in the magnetostriction. For example, the frequency doubling effect is no longer given above 60 Hz according to the measurement results shown in [28] for Metglas 2605SA1 as-cast ribbon. Since a capacitor in series of the winding is used during the core measurement presented in this paper, there is no dc magnetization. Therefore, it is assumed that the odd harmonics, which appear in the measured vibration velocity spectrum, are induced due to the asymmetrical magnetostriction at high frequency.

2) Winding: In case of the winding, a dc current (e.g., in case of short-circuit fault) can lead to a Lorentz force and a vibration harmonic at the excitation frequency [29]. Higher order odd harmonics of the winding vibration can be induced if there is also higher order even harmonics in the current. This is caused due to the fact that the Lorentz force contains harmonics not only at the double frequency of the current harmonics but also at the sum and difference frequencies of each two current harmonics [30].

Considering the vibration and acoustic noise measured on the winding in this paper (see Fig. 21), the odd harmonic at the excitation frequency (4 kHz) is also present. Due to the series capacitor, there is neither dc current nor even harmonics flowing through the winding. Consequently, it is assumed that this odd harmonic in the vibration and the sound pressure spectra is not excited by electromagnetic force. It is also reported in [9] that the winding vibration contains odd harmonic at the excitation frequency, and its amplitude can be even higher than the harmonic at twice of excitation frequency (as shown in this case).

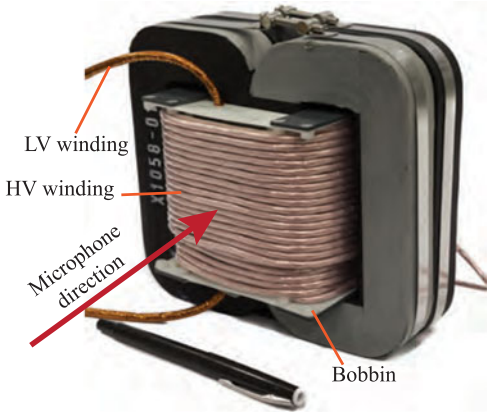

Fig. 22. Transformer prototype with four sets of VITROPERM 500F T60102-L2157-W159 uncut cores, turns ratio $N_{\mathrm{HV}} : N_{\mathrm{LV}} = 40{:}15$, HV winding with 620×0.1 mm Litz-wire, LV winding with 4000×0.05 mm Litz-wire.

This harmonic is explained to be caused by nonlinear mechanical behavior and is related to the tightness of the winding. In fact, the cause of odd harmonics in winding vibration signal due to mechanical fault has been considered for diagnosis purposes, especially for detecting the winding deformation or looseness [26], [31], [32]. In normal condition, the measured vibration signal on the winding only contains even harmonics. However, if the winding is deformed, odd harmonics may appear, which is experimentally shown in [26] and [32]. Nevertheless, the mechanisms of odd harmonics in vibration signal due to mechanical nonlinearity is not well explained in these publications.

VI. Acoustic Measurement of Transformer

To evaluate the acoustic noise emission of MFTs, a prototype transformer with shell type structure as shown in Fig. 22 has been built. The transformer consists of four sets of VITROPERM 500F uncut cores. Since only one oval core is available, the rectangular cores are used instead, which is the same one used for vibration and acoustic measurements as mentioned before. The HV winding consists of 620×0.1 mm Litz-wire with 40 turns whereas the LV winding has 15 turns of 4000×0.05 mm Litz-wire. To facilitate the construction of the winding, a plastic bobbin is printed with a three-dimensional printer. Since the magnetic core is uncut, the bobbin has to be produced as two halves so that they can be mounted around the central limb of the core.

The transformer is operated with a single-active-bridge converter (SABC) as shown in Figs. 23 and 24. With this configuration, similar operating conditions (voltage/current waveforms) for the transformer are obtained as with a dual-active-bridge converter (DABC) operated by phase-shift modulation. The operation of the SABC is based on the duty cycle modulation, where the transferred power is adjusted by modifying the voltage-second product applied on the LV windings. The converter is supplied with 400-V dc voltage and operated at a fixed switching frequency of 4 kHz. The output voltage is measured and regulated to be 800 V by a proportional-integral (PI)-controller implemented on a field programmable gate array (FPGA) board.

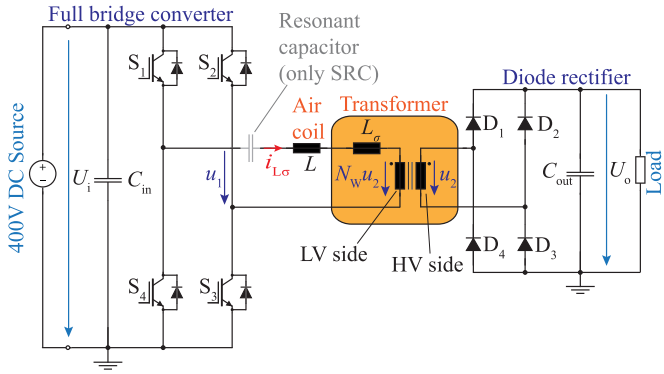

Fig. 23. Schematic of the SABC/SRC converter.

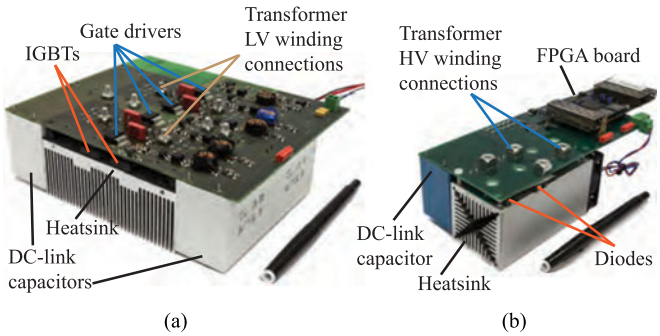

Fig. 24. Implemented prototype of full-bridge converter and diode rectifier. (a) Full-bridge converter. (b) Diode rectifier.

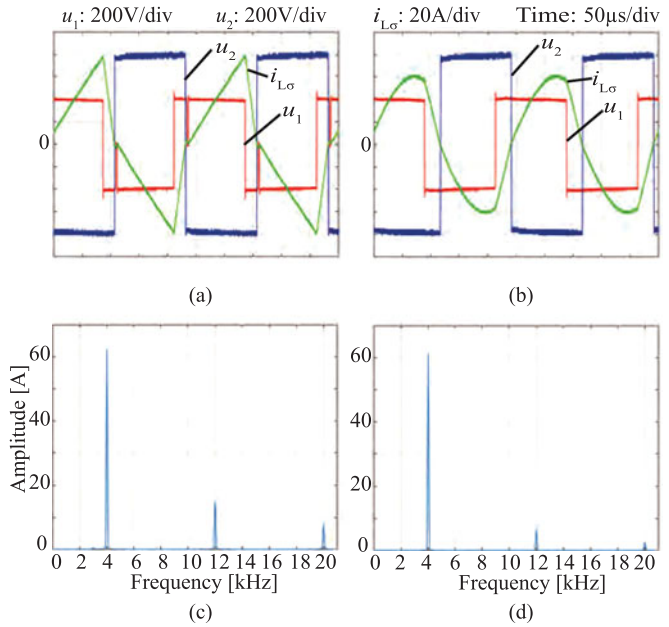

Fig. 25. Measured waveforms of transformer voltage/current operating at 10 kW as in SABC and SRC. The first three harmonics of the current in the LV winding for both cases are also shown. (a) SABC waveforms. (b) SRC waveforms. (c) Current harmonics of SABC. (d) Current harmonics of SRC.

In order to limit the maximum transferred power, an additional inductor built as an air coil with the same Litz-wire used for the LV winding is connected in series to the LV side. In this way, the maximal value for the voltage-second product can be achieved at lower power level so that the maximal excitation of the core can be obtained with the given voltage. Due to the required interlocking time for the switches, the voltage-second product is limited to approximately 98% of the theoretical maximal value.

For comparison between the SABC and the series resonant converter (SRC), a capacitor bank with a total capacitance of 5.1 μF is also built and connected in series to the air coil. In this case, the SABC is operated as an SRC. Accordingly, the inductance of the air coil is adapted so that by operating the SRC at the same frequency, output power and output voltage, the voltage-second product also reaches approximately the same value as in the case of the SABC.

In Fig. 25(a) and (b), the current and voltage waveforms of the transformer for the SABC and the SRC under the operating conditions described above are shown. The transferred power is approximately 10 kW and in both cases the calculated peak flux density in the transformer core is approximately 0.5 T. The voltages u_1 and u_2 are measured at the locations as shown in Fig. 23. It can be seen that the peak current flowing through the LV winding is approximately 80 A for the SABC whereas it is around 60A for the SRC. In Fig. 25(c) and (d), the first three harmonics of the current in the transformer LV winding are shown, where the first harmonic in both cases are quite similar whereas the third and the fifth harmonics for the SRC are lower than for the SABC due to the more sinusoidal shape.

With the operation conditions given above, the acoustic measurement of the transformer is performed with the microphone located 1 m away from the surface of the transformer and the measurement direction is shown in Fig. 22. Due to the required source and load for the test setup, the measurement is not performed in the anechoic room. During the measurement, there are influences from other sound sources, such as the cooling fans of the converter and the dc sources. In Fig. 26, the measured sound pressure spectra of the transformer for both the SABC and the SRC are shown. As reference, the background noise is also measured, where the dc sources and the cooling fans of the converter are also turned ON during the measurement. It can be seen that the transformer generally induces additional noise above the operating frequency. The A-weighted SPL is increased by approximately 4–5 dBA compared to the background noise. For the SABC and the SRC, the transformer noise is quite similar with a difference of less than 1 dBA. This can be expected by the similar excitations of the core and amplitudes of the main current harmonic (4 kHz). Although in case of the SABC, the current has higher third and fifth harmonics, the induced noise due to these harmonics mainly at doubled frequencies (24 kHz and 40 kHz) are already beyond the audible range, and therefore, have minor contribution to the acoustic noise.

To compare the contribution of the transformer noise from the core and the winding, the oval uncut core is measured again. During this measurement, only the ac amplifiers for supplying the excitation current is turned ON. In this case, the measured frequency spectra of the background noise and core noise are shown in Fig. 27(a) and (b), respectively. The core is excited by 4 kHz sinusoidal current to a flux density level

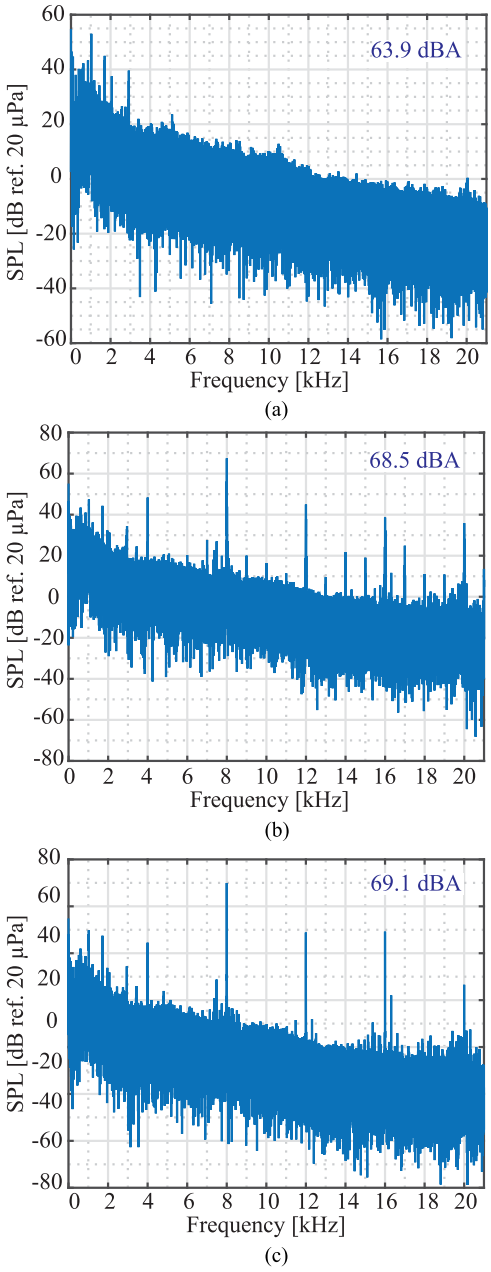

Fig. 26. Measured SPL frequency spectra of transformer and background noise (with dc sources and converter cooling fans turned ON). (a) Background. (b) Transformer (SABC). (c) Transformer (SRC).

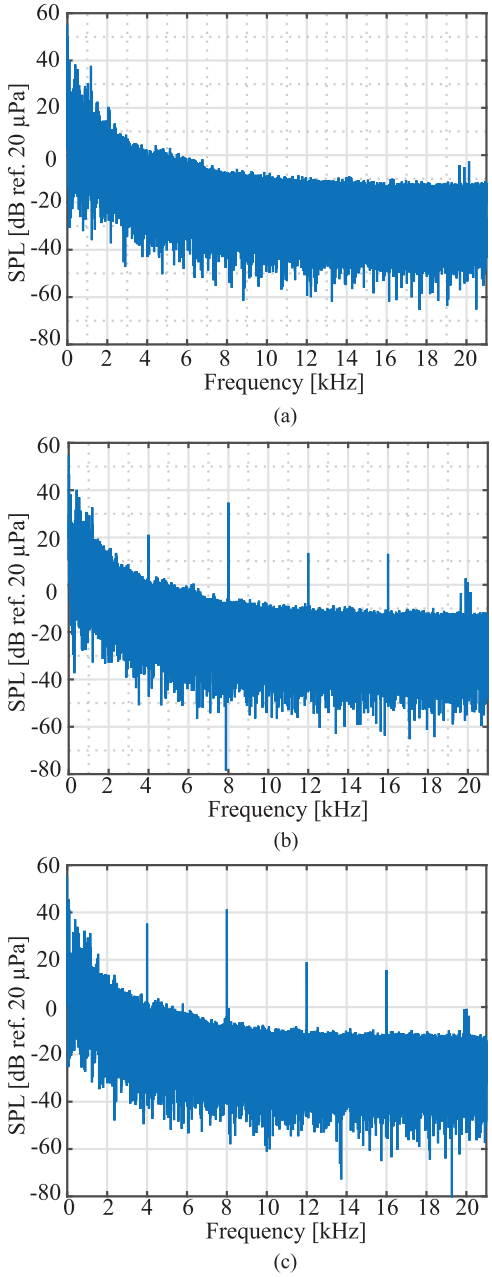

Fig. 27. Measured SPL frequency spectra of oval core, single-layer winding, and background noise (with dc sources and converter cooling fans turned OFF). (a) Background. (b) Oval uncut core. (c) Winding (22 turns).

of 1.0 T (measured toward the front surface). It can be seen that even at this high induction level, the highest amplitudes of the core noise harmonic is still lower than the amplitudes of the background noise in the low-frequency range. For further comparison, a single-layer winding with 22 turns fed by 50 A peak sinusoidal current is measured and the noise spectrum is shown in Fig. 27(c). This winding is built by the same Litz-wire used for the HV winding of the transformer and has the same size. By comparing the amplitudes of the noise harmonics, it can be seen that the winding noise has higher amplitudes than the core noise. In case of the transformer, both LV and HV windings contribute to the noise and the current amplitude in the HV winding is even higher than the measured current in the single-layer winding. Furthermore, the flux density in the transformer core is only half of the flux density in the measured oval core. Therefore, the transformer core is expected to have lower noise than the measured oval core whereas the transformer winding is expected to generate more noise than the single-layer winding. As a result, it can be concluded that the measured transformer noise is mainly caused by the winding vibration whereas the core vibration only has a minor contribution due to the small magnetostriction and Maxwell force.

The acoustic noise of a transformer based on Fe-based amorphous core has been reported, where the sound power level of

the transformer excited to the flux density level of 0.45 T is measured to be over 100 dB [33]. This is equivalent to the SPL of over 90 dB if measured at 1 m from the transformer as in the case of this paper. For the transformer in this paper, the measured SPL is more than 20 dB lower compared with the transformer reported in [33]. Therefore, it can be concluded that by using the nanocrystalline uncut core, the acoustic noise emission of the transformer can be significantly reduced. In this case, the core noise is relative low and the winding noise has a dominant contribution to the total transformer noise.

VII. Conclusion

In this paper, the origins of acoustic noise in transformers for medium-frequency, high-power applications are investigated. The work is based on vibration and acoustic measurements of magnetic cores focusing on the electromagnetic origins, i.e., magnetostriction and magnetic forces.

The comparison between cut and uncut cores shows that air gaps introduce excessive magnetic forces which induce large vibrations near the air gap region and enhance the vibrations at other parts of the core due to the mechanical contact. As a result, the cut core has much higher noise emission compared with its uncut counterpart. The frequency spectra of the measured surface velocities show that the harmonic of vibration at twice of the excitation frequency is dominant. Therefore, particular attention needs to be paid to avoid the coincidence of the double of the excitation frequencies with the eigenfrequencies of the core since these frequencies are also in the operating frequency range as shown by the measurement (see Fig. 9).

Considering the core noise, the investigation is focusing on the influence of core material properties and geometric shape. Several magnetic materials with interest for medium-frequency applications are compared. Ferrite features low noise but its application for MFT operated at a few kilo Hertz with high power density requirement is limited due to the low saturation flux density. For the Fe-based amorphous alloys, the relative strong vibration and accordingly the large acoustic noise emission of this material due to large magnetostriction is confirmed by measurement results. On the contrary, the Co-based amorphous alloy has near-zero magnetostriction that results in much lower acoustic noise compared to the Fe-based amorphous alloy. Both vibration and acoustic measurements confirm that the nanocrystalline material is superior for low noise transformer design. Moreover, this material is also advantageous in terms of power density and efficiency compared to other core materials, which makes nanocrystalline alloy the most suitable one for highly efficient, compact, and quiet MFT design.

Vibration measurements indicate that the direction perpendicular to the lamination layers of tape wound cores has larger vibration and more noise emission compared to the direction parallel to the lamination layers. In case of the rectangular core, the large curvature at the corners results in intensive vibrations at the surfaces near the corners. On the other hand, the vibration of a ring core is much weaker due to more homogeneously distributed magnetic flux and therefore the magnetic forces and magnetostrictive strains. The oval core is a combination of the two shapes and its acoustic performance is in between, which is a good compromise for low acoustic noise and high power density.

The comparison between the core noise and the winding noise indicates that the winding has a major contribution to acoustic noise if the core vibration is weak (e.g., in case of an uncut core with low magnetostriction and/or low induction level) and the current flowing through the winding is relative small. Otherwise, the core noise is usually more significant than the winding noise.

Finally, a transformer based on nanocrystalline uncut cores with rectangular shape is built, on which the acoustic measurement is performed where the transformer is operated both as SABC and SRC. The results show that under the excitation of a rectangular voltage, the higher-order harmonics in the frequency spectrum of acoustic noise are more significant than in the case of a sinusoidal excitation. In case of the SABC, the triangular-shaped current has larger higher-order harmonics compared with the more sinusoidal current of the SRC. However, the transformer noise is similar in both cases due to the same excitation voltage and similar amplitudes of the main current harmonic. The measurement results show that in case the magnetic core is uncut and has a low magnetostriction, the winding vibration induced by the Lorentz force due to the high current has a more significant contribution to the acoustic noise of transformer, which confirms the measurement results obtained from the core and winding measurements. Compared with a transformer built with Fe-based amorphous cut cores reported in the literature, the transformer measured in this paper is proved to have much less acoustic noise emission.

Based on these results, the effort to reduce the acoustic noise emission of such a transformer should be put on the winding. It is expected that by suitable mechanical damping or potting the winding with epoxy, the winding vibration can be effectively reduced. To verify this, further investigation is necessary, which is out of the scope of this paper.

Acknowledgment

The authors would like to thank VACUUMSCHMELZE GmbH for providing the core samples and valuable information about the core materials.

References

[1] J. W. Kolar and G. I. Ortiz, "Solid-state-transformers: Key components of future traction and smart grid systems," in *Proc. Int. Power Electron. Conf.*, 2014.

[2] P. Shuai and J. Biela, "Design and optimization of medium frequency, medium voltage transformers," in *Proc. 15th Eur. Conf. Power Electron. Appl.*, 2013, pp. 1–10.

[3] A. Belahcen, "Magnetoelasticity, magnetic forces and magnetostriction in electrical machines," Ph.D. dissertation, Helsinki Univ. Technol., Espoo, Finland, 2004.

[4] J. Roivainen, "Unit-wave response-based modeling of electromechanical noise and vibration of electrical machines," Ph.D. dissertation, Helsinki Univ. Technol., Espoo, Finland, 2009.

[5] M. van der Giet, "Analysis of electromagnetic acoustic noise excitations: A contribution to low-noise design and to the auralization of electrical machines," Ph.D. dissertation, RWTH-Aachen Univ., Aachen, Germany, 2011.

[6] B. Weiser, H. Pfützner, and J. Anger, "Relevance of magnetostriction and forces for the generation of audible noise of transformer cores," *IEEE Trans. Magn.*, vol. 36, no. 5, pp. 3759–3777, Sep. 2000.
[7] R. S. Masti, W. Desmet, and W. Heylen, "On the influence of core laminations upon power transformer noise," in *Proc. Int. Conf. Noise Vib. Eng.*, 2004, pp. 3851–3862.
[8] A. Moses, P. Anderson, T. Phophongviwat, and S. Tabrizi, "Contribution of magnetostriction to transformer noise," in *Proc. 45th Int. Univ. Power Eng. Conf.*, 2010, pp. 1–5.
[9] O. Barre, B. Napame, M. Hecquet, and P. Brochet, "Acoustic noise emitted by passive components in magnetic devices and design of a low-noise industrial inductor," *COMPEL: Int. J. Comput. Math. Elect. Electron. Eng.*, vol. 27, no. 5, pp. 1053–1068, 2008.
[10] S. Schmitt, "Acoustic noise of sheeted electrical steel inductors in PWM operation—causes and mitigation," in *Proc. 13th Eur. Conf. Power Electron. Appl.*, 2009, pp. 1–8.
[11] J. Mühlethalter, M. Schubiger, U. Badstübner, and J. W. Kolar, "Acoustic noise in inductive power components," in *Proc. 15th Eur. Conf. Power Electron. Appl.*, 2013, pp. 1–8.
[12] P. Jang and G. Choi, "Acoustic noise characteristics and magnetostriction of Fe-Si powder cores," *IEEE Trans. Magn.*, vol. 48, no. 4, pp. 1549–1552, Apr. 2012.
[13] Y. Gao *et al.*, "Design of a reactor driven by inverter power supply to reduce the noise considering electromagnetism and magnetostriction," *IEEE Trans. Magn.*, vol. 46, no. 6, pp. 2179–2182, Jun. 2010.
[14] Y. Gao, M. Nagata, K. Muramatsu, K. Fujiwara, Y. Ishihara, and S. Fukuchi, "Noise reduction of a three-phase reactor by optimization of gaps between cores considering electromagnetism and magnetostriction," *IEEE Trans. Magn.*, vol. 47, no. 10, pp. 2772–2775, Oct. 2011.
[15] M. Rossi and J. Le Besnerais, "Vibration reduction of inductors under magnetostrictive and Maxwell forces excitation," *IEEE Trans. Magn.*, vol. 51, no. 12, pp. 1–6, Dec. 2015.
[16] A. Kelley, "Measurement of spacecraft power transformer acoustic noise," *IEEE Trans. Magn.*, vol. 26, no. 1, pp. 281–289, Jan. 1990.
[17] Y. G. Yao, T. Phway, A. Moses, and F. Anayi, "Magneto-mechanical resonance in a model 3-phase 3-limb transformer core under sinusoidal and PWM voltage excitation," *IEEE Trans. Magn.*, vol. 44, no. 11, pp. 4111–4114, Nov. 2008.
[18] Y.-H. Chang, C.-H. Hsu, H.-L. Chu, and C.-P. Tseng, "Magnetomechanical vibrations of three-phase three-leg transformer with different amorphous-cored structures," *IEEE Trans. Magn.*, vol. 47, no. 10, pp. 2780–2783, Oct. 2011.
[19] Y.-H. Chang, C.-H. Hsu, H.-W. Lin, and C.-P. Tseng, "Reducing audible noise for distribution transformer with HB1 amorphous core," *J. Appl. Phys.*, vol. 109, no. 7, 2011, Art. no. 07A318.
[20] P. Shuai and J. Biela, "Investigation of acoustic noise sources in medium frequency, medium voltage transformers," in *Proc. 16th Eur. Conf. Power Electron. Appl.*, 2014, pp. 1–11.
[21] P. Shuai and J. Biela, "Impact of core shape and material on the acoustic noise emission of medium frequency, medium voltage transformers," in *Proc. 17th Eur. Conf. Power Electron. Appl.*, 2015, pp. 1–11.
[22] Z. Ren, "Comparison of different force calculation methods in 3D finite element modelling," *IEEE Trans. Magn.*, vol. 30, no. 5, pp. 3471–3474, Sep. 1994.
[23] R. Hilzinger and W. Rodewald, *Magnetic Materials - Fundamentals, Products, Properties, Applications*. Erlangen, Germany: Publics Publ., 2013.
[24] J. H. Harlow, *Electric Power Transformer Engineering*. Boca Raton, FL, USA: CRC Press, 2012.
[25] B. Garcia, J. C. Burgos, and A. M. Alonso, "Transformer tank vibration modeling as a method of detecting winding deformations-part I: Theoretical foundation," *IEEE Trans. Power Del.*, vol. 21, no. 1, pp. 157–163, Jan. 2006.
[26] K. Hong and H. Huang, "Power transformer fault diagnosis based on vibration correlation analysis," in *Proc. Int. Mech. Eng. Congr. Expo.*, 2014, p. V013T16A029.
[27] S. Wada and T. Yagisawa, "On the loss and magnetostriction of electrical steel for the dc superposed flux alternation," *J. Magn. Magn. Mater.*, vol. 19, no. 1–3, pp. 39–41, 1980.
[28] S. U. Jen, C. C. Liu, H. R. Lin, and S. H. Chou, "Frequency dependence of the magnetostrictive phenomenon in metglas 2605SA1 ribbon: A minor-loop case," *AIP Advances*, vol. 4, no. 127140, pp. 1–4, 2014.
[29] Y.-Q. Tang, J.-Q. Qiao, and Z.-H. Xu, "Numerical calculation of short circuit electromagnetic forces on the transformer winding," *IEEE Trans. Magn.*, vol. 26, no. 2, pp. 1039–1041, Mar. 1990.
[30] M. Ertl and S. Voss, "The role of load harmonics in audible noise of electrical transformers," *J. Sound Vib.*, vol. 333, no. 8, pp. 2253–2270, 2014.
[31] Y. Shao, H. Guan, Y. Zhang, Z. Jin, and Z. Rao, "A vibration method for identifying the looseness of windings for large power transformers," in *Proc. 4th Int. Conf. Signal Process. Syst.*, 2012, pp. 176–182.
[32] H. Ma, N. Jiang, C. Wang, and Z. Geng, "Improved power transformer winding deformation fault diagnosis method," *Appl. Mech. Mater.*, vol. 666, pp. 149–153, 2014.
[33] I. Villar, "Multiphysical characterization of medium-frequency power electronic transformers," Ph.D. dissertation, EPFL, Switzerland, 2010.

Peng Shuai (S'13) received the B.Eng. degree from Zhejiang University, Hangzhou, China, in 2006, and the M.Sc. degree from RWTH Aachen University, Aachen, Germany, in 2009, both in electrical engineering. He is currently working toward the Ph.D. degree in electrical engineering at the Laboratory for High Power Electronic Systems, Swiss Federal Institute of Technology Zurich, Zurich, Switzerland.

From 2008 to 2009, he was with Corporate Research Center of ABB Switzerland, Ltd., Baden-Dättwil, Switzerland, working on his Master thesis. From 2010 to 2011, he worked in the R&D Center of Huawei Technologies Sweden AB, Kista, Sweden, as a Development Engineer for power electronics. His current research interests include solid-state transformer, optimization of transformer, magnetic materials for medium frequency applications, and acoustic noise emission of magnetic components.

Juergen Biela (S'04–M'06–SM'16) received the Diploma (Hons.) degree in electrical engineering from Friedrich-Alexander Universität Erlangen-Nürnberg, Nuremberg, Germany, in 1999, and the Ph.D. degree in electrical engineering from the Swiss Federal Institute of Technology (ETH) Zurich, Zurich, Switzerland, in 2006.

In 2000, he joined the Research Department, Siemens A&D, Erlangen, Germany, where he has been involved in inverters with very high switching frequencies, SiC components, and EMC. In 2002, he joined the Power Electronic Systems Laboratory, ETH Zurich, as the Ph.D. student focusing on optimized electromagnetically integrated resonant converters. From 2006 to 2007, he was a Postdoctoral Fellow with the Power Electronic Systems Laboratory, and a Guest Researcher with the Tokyo Institute of Technology, Tokyo, Japan. From 2007 to 2010, he was a Senior Research Associate with the Power Electronic Systems Laboratory. Since 2010, he has been an Associate Professor of high-power electronic systems with ETH Zurich. His current research interests include the design, modelling, and optimization of power factor correction, dc-dc, and multilevel converters with an emphasis on passive components, the design of pulsed-power systems, and power electronic systems for future energy distribution.